IEEE Access
Multidisciplinary ⋮ Rapid Review ⋮ Open Access Journal

Received 17 August 2023, accepted 15 September 2023, date of publication 28 September 2023,
date of current version 11 October 2023.

Digital Object Identifier 10.1109/ACCESS.2023.3320582

RESEARCH ARTICLE

Three Level Bidirectional DC/DC Intelligent Control Technology for Photovoltaic Charging Station of Electric Vehicle Combined With SVPWM Algorithm

YANSHENG HUANG[1], SHUTING LIN[1], AND HAIJUN MO[2]
[1]School of Energy Power and Environmental Engineering, Guangxi Electrical Polytechnic Institute, Nanning 530299, China
[2]School of Mechanical Engineering, Guangxi University, Nanning 530299, China

Corresponding author: Haijun Mo (mhj9801@sina.com)

ABSTRACT Due to new energy electric vehicle market developing rapidly, a series of energy supply problems in the charging system urgently need to be solved. The two subsystems of this new energy photovoltaic charging station system are studied respectively. Firstly, the topology equivalent circuit diagram of a three-level pulse width modulation rectifier is proposed. And a simplified space vector pulse width modulation algorithm is applied to the control of the current inner loop and voltage outer loop of three-level AC/DC. A three-level bidirectional DC/DC converter was introduced, its power characteristics and implementation conditions of soft switching were analyzed, and a phase shift modulation method was proposed to achieve its intelligent control. The results indicate that in the dynamic performance analysis of the simplified space vector pulse width modulation algorithm, the phase of phase A current and voltage are in a synchronous state before and after adding a load. After adding the load, the A-phase voltage remained stable at 300V, but its maximum current increased from 80A to 150A. At the same time, the maximum value of three-phase current suddenly changed from 80A to 150A after the load was added, and subsequently stabilized at about 150A. In the power characteristic experiment of a three-level bidirectional DC/DC converter, when the set current Iset is positive, the current value of the input current IinF of the primary bridge arm stabilizes at 11.5A around 0.025 seconds. When the set current Iset is negative, the current value of the input current IinF of the primary bridge arm stabilizes at −11.5A around 0.020s. This shows that the three-level bidirectional DC/DC converter can convert the photovoltaic system's output voltage to the voltage requirements on DC side of the inverter. The three-level AC/DC and three-level bidirectional DC/DC converters used in this study have significant performance advantages, providing reliable technical support for the photovoltaic charging station technology of modern new energy electric vehicles.

INDEX TERMS SVPWM algorithm, photovoltaic charging station, three level, AC/DC, bidirectional DC/DC converter, intelligent control.

I. INTRODUCTION

The modern technology developing has led to an increasing demand for electric energy among humans. However, the current electricity supply energy mainly consists of non renewable fossil fuels, which can cause environmental damage during use and seriously endanger the development of human society [1], [2]. Hydroelectric power generation faces the problem of unequal allocation of power generation resources, while wind power generation faces the problem of low power generation stability. To meet the sustainable development of humanity, resources, and the environment, it is necessary to construct a new energy structure system. Solar energy is a clean and resource rich new energy source,

The associate editor coordinating the review of this manuscript and approving it for publication was Bin Xu.

which is currently widely used in the energy supply of new energy vehicles. Among them, the coverage and quantity of electric vehicle charging devices have become the driving force for maintaining their sustainable development [3]. The current grid level cannot meet the charging station demand of new energy vehicles, so the electric energy generated by the solar photovoltaic system can be used as the energy source of the charging device. But when the microgrid composed of photovoltaic charging stations is connected to the power grid on a large scale, its impact on the power grid is not clear enough, so it needs to be evaluated [4]. The research adopts the photovoltaic DC/DC in the photovoltaic charging station (PCS) system to convert the output voltage into a voltage form that matches DC side voltage of the inverter, and converts the output energy into current electricity to be transmitted to the power grid. At the same time, AC/DC energy storage system is used to balance the voltage on DC bus, and bidirectional DC/DC is used to control the charging and discharging of electric Automotive battery. The advantage of the research lies in addressing the low energy efficiency issues faced by the power control technology of traditional electric vehicle photovoltaic charging stations. The proposed method adopts more advanced topology and control methods, thereby improving energy conversion efficiency and charging speed, while reducing energy loss and system costs. These advantages make electric vehicle charging stations more reliable and efficient, and are of great significance for sustainable development and energy management [5]. The research content consists of four parts. Firstly, a review was mainly conducted on microgrid technology and PCS technology. Secondly, research was conducted on the three-level AC/DC and three-level bidirectional DC/DC of PCS subsystem. The first section introduces a Pulse Width Modulation (PWM) rectifier structure model of three-level AC/DC. And a simplified Space Vector Pulse Width Modulation (SVPWM) algorithm was used to calculate the three-level action time and applied to the control of the current inner loop and voltage outer loop. Secondly, the power flow characteristics of three-level bidirectional DC/DC converters and the implementation conditions of soft switching are mainly introduced. The third part analyzes the experimental results of the application characteristics of simplified SVPWM in three-phase PWM rectifiers, and analyzes the performance and soft switching implementation of three-level bidirectional DC/DC converters. Finally, a summary and discussion of the experiment were conducted, and future prospects were proposed.

II. RELATED WORKS

Microgrid technology can effectively solve the problem of power supply systems struggling to meet the needs of distributed power sources. M. Mansoor and other researchers designed a mixed integer linear programming model of hydrogen energy system for the optimal planning problem of microgrid technology. At the same time, they used the microgrid laboratory to analyze real cases. The case fully considers the electrolysis process and seasonal storage of hydrogen production. The results confirm that the low emission hydrogen migration framework is achieved through the high share of renewable energy in the microgrid and seasonal hydrogen storage [6]. Z. Huang et al found that vanadium redox flow battery can be well applied to large-scale electrochemical energy storage. Therefore, they proposed that a microgrid composed of photovoltaic, VRFB, and wind renewable energy is an effective method to solve the randomness problem of renewable energy. The results confirm that this scheme effectively improves the renewable energy performance in microgrids [7]. F. Yang and other scholars have introduced a new EMS method to implement flexible time frame DER plans and EDs based on single period OPF for the improvement of microgrid technology. Among them, FTF DER enables microgrids to fully utilize the latest renewable energy, and ED based on single period OPF effectively achieves the integration of microgrid operation constraints. The results confirm that the proposed new microgrid EMS technology has strong feasibility [8]. L. Yavuz's team has proposed virtual power plant technology to address the issues of low efficiency and low power quality that renewable energy brings to the operation of the power system. This technology is closely related to most components in the power system, including Electric power transmission operators, distribution system operators, distributed generation, etc. The results confirm that this technology can effectively improve the power grid's stability and reliability [9]. S. Chandak et al. explored the integration of microgrids with existing power systems and their operational characteristics, and proposed control strategies based on microgrid technology. The results confirm that this scheme can effectively improve the overall performance of the microgrid and achieve smooth access of the microgrid in the power system [10]. T. M. Masaud et al. found that determining the battery storage system's optimal size in microgrid system design is a challenging issue. Therefore, this team introduced a two-stage approach to determine the optimal size of the battery storage system. In the first stage, the mixed integer linear programming algorithm is designed, and in the second stage, the battery life is estimated on this basis. The numerical simulation results indicate that this scheme has strong feasibility [11].

PCS technology is currently widely used in the energy supply of electric vehicles. Electric vehicles have problems such as slow charging time, insufficient charging stations, and unstable power grids during peak hours. In response, P. Prem et al. proposed a high gain, fast charging DC/DC converter and an electric vehicle charging station based on solar photovoltaic power generation. And they used MATLAB to verify the performance of the proposed converter and its control algorithm. The results confirm that the converter meets the power quality standard, and the solar photovoltaic Charging station meets DC charging standard [12]. There are energy management issues with distributed electric vehicle charging stations for solar photovoltaic systems and energy storage systems. In this regard,

M. Shin et al. proposed a new multi intelligence Deep reinforcement learning method. Unlike traditional methods, this method can calculate the scheduling schemes of multiple electric vehicle charging stations in a distributed manner and simultaneously process dynamic data during operation. These results confirm that this method can reduce the operating costs of electric vehicle charging stations effectively [13]. S. Praveenkumar et al. found that India's power generation and road transportation have caused significant fossil fuel consumption. Therefore, they evaluated the role of solar energy technology and power plants in electricity and hydrogen production. The results confirm that five cities in India can generate approximately 25 gigawatts of electricity per year, and it is necessary to develop different optimized configurations in different regions [14]. S. M. Shariff's team found it difficult to carry out large-scale sustainable deployment of renewable energy based transportation systems. Therefore, they applied modern solar energy controlled by Type 1 vehicle connectors to Level 2 electric vehicle charging stations. At the same time, a design model was developed in the MATLAB environment and the controller circuit was simulated in the PROTEUS software. The results confirmed that the design can provide good guidance for the large-scale deployment of renewable energy [15]. A. Sierra et al. validated the feasibility of using local battery storage for photovoltaic charging stations in electric vehicles and designed a simulation model. This model is based on the share of photovoltaic energy and estimates the energy balance, annual energy cost, and cumulative carbon dioxide emissions of the system under different conditions. The results confirmed that the electric vehicle charging system located in commercial or office parking lots is effective [16]. To design a truly efficient EMS for photovoltaic auxiliary charging stations, researchers such as M. Zand proposed solid-state transformers for solar power plant design and an energy management solution for solid-state transformers. The results confirm that this energy management scheme has achieved certain results in actual energy management, and it effectively improves the operation of charging stations, enabling continuous power supply [17]. A. Verma et al. conducted relevant research on multi-mode operation of battery, Photovoltaic system, power grid and Diesel generator charging station. In this charging station, its control design is to obtain power mainly from Photovoltaic system and battery. And the operation mode of distributed generator sets makes the power generated 33% more than its Nameplate capacity. The results confirm that the charging station meets the standard under all operating modes, and the total harmonic distortion rate of current and voltage is less than 5% [18].

In summary, many domestic and foreign researchers have conducted extensive research on microgrid technology and PCS technology, and have achieved corresponding results. However, there is a lack of research on the various subsystems and corresponding control strategies of photovoltaic charging systems. Therefore, this article investigates the three-level AC/DC and three-level bidirectional DC/DC of PCS subsystem. And the intelligent control technology was discussed, with the aim of promoting the further development of modern new energy vehicle PCS technology.

III. THREE LEVEL AC/DC AND BIDIRECTIONAL DC/DC OF PCS SUBSYSTEM

In the first section of this chapter, three-level AC/DC in PCS subsystem is introduced, and the topology equivalent circuit of the diode clamped three-level PWM rectifier is introduced. The influence of power transistor on the input current of AC side under different switching states is explained in detail. Andaction time of each vector and the control effect of SVPWM are explained. The second section mainly introduces the topology and characteristic analyzingof this three-level bidirectional DC/DC converter, and introduces the implementation conditions of soft switching in the system circuit. And different control methods were discussed.

A. THREE LEVEL AC/DC BASED ON SVPWM

The photovoltaic charging system is mainly composed of bidirectional Charging station and photovoltaic power generation system. Among them, photovoltaic DC/DC is mainly responsible for converting the output voltage of photovoltaic system to DC side voltage of the inverter. DC/AC is an inverter structure that mainly converts the electrical energy output by DC/DC into current and inputs it into the power grid. And it also plays a role in balancing the power of DC bus. AC/DC is an energy storage system with a bidirectional power flow structure. The system can include a front and rear two-stage structure. The front stage mainly adopts an inverter structure, which can work in both rectified and inverter states, and plays a role in balancing DC bus voltage. The latter stage of AC/DC is bidirectional DC/DC, which mainly plays a charging and discharging control role for EV batteries [19].

Multilevel rectifiers are currently widely used in power systems. Unlike two-level rectifiers, three-level rectifiers have a larger number of power switches and a more complex topology of the main circuit. In a three-level rectifier, four power switches are used for each phase of the bridge arm. This results in each power switch having a voltage of only 1/2 of DC side voltage when the level is in the off state, effectively reducing the cost of selecting switch power. Based on this advantage, three-level rectifiers can adapt to high-voltage and high-frequency situations, with small waveform distortion rate, low switch consumption, and reduced pollution to the power grid. The multi-level type used in the study is diode clamped, which has a relatively simple control method and can achieve bidirectional energy flow. Figure 1 shows the topology equivalent circuit of a diode clamped three-level PWM rectifier.

Equation (1) is the switching function ofpower switch of a three-level PWM rectifier.

$$S_i = \begin{cases} -1, \text{ Power tube } T_{i3} \text{ and } T_{i4} \text{ conduction} \\ 0, \text{ Power tube } T_{i2} \text{ and } T_{i3} \text{ conduction} \\ 1, \text{ Power tube } T_{i1} \text{ and } T_{i2} \text{ conduction} \end{cases} \quad (1)$$

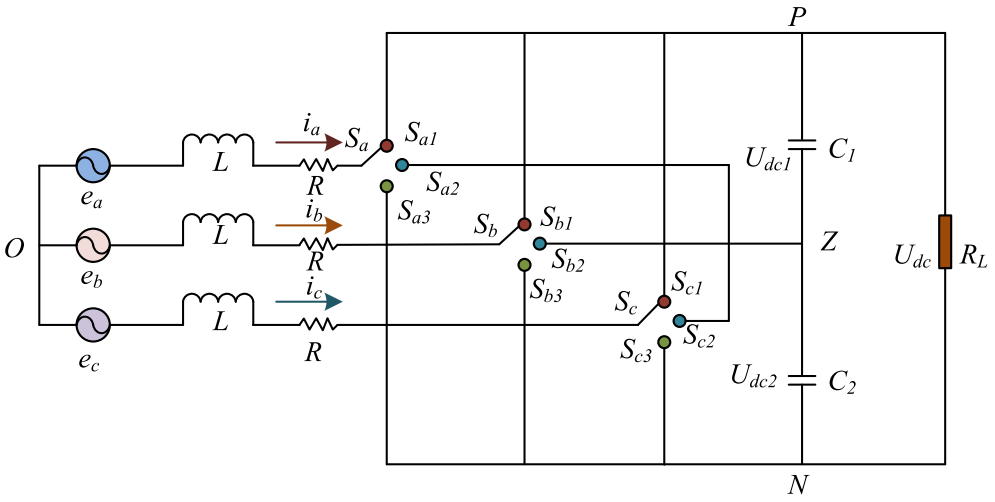

FIGURE 1. Equivalent circuit diagram of the main circuit of a two-level PWM rectifier.

In equation (1), $i = a, b, c$. By using equivalent circuits to explain it, equation (2) can be obtained.

$$S_i = \begin{cases} -1, \mathrm{S_{i1}} = 0, \mathrm{S_{i2}} = 0, \mathrm{S_{i3}} = 1 \\ 0, \mathrm{S_{i1}} = 0, \mathrm{S_{i2}} = 1, \mathrm{S_{i3}} = 0 \\ 1, \mathrm{S_{i1}} = 0, \mathrm{S_{i2}} = 0, \mathrm{S_{i3}} = 1 \end{cases} \tag{2}$$

According to Kirchhoff's voltage and current law, a three-phase voltage equation on AC side of the rectifier can be obtained in Formula (3).

$$\begin{cases} L\dfrac{di_a}{dt} = e_a - S_{a1}U_{dc1} - S_{a3}U_{dc2} - U_{OZ} - i_aR \\ L\dfrac{di_b}{dt} = e_b - S_{b1}U_{dc1} - S_{b3}U_{dc2} - U_{OZ} - i_bR \\ L\dfrac{di_c}{dt} = e_c - S_{c1}U_{dc1} - S_{c3}U_{dc2} - U_{OZ} - i_cR \end{cases} \tag{3}$$

In equation (3), e stands for the power supply voltage, i stands for the current, L stands for the inductance, U stands for the voltage between two points, and R stands for the resistance. Among them, equation (4) stands for the relationship between i and e.

$$\begin{cases} e_a + e_b + e_c = 0 \\ i_a + i_b + i_c = 0 \end{cases} \tag{4}$$

By introducing equation (4) into equation (3), equation (5) can be obtained.

$$U_{OZ} = \frac{(S_{a3} + S_{b3} + S_{c3})U_{dc2}}{3} - \frac{(S_{a1} + S_{b1} + S_{c1})U_{dc1}}{3} \tag{5}$$

Equation (6) is the current equation for node P.

$$C_1\frac{dU_{dc1}}{d_t} = S_{a1}i_a + S_{b1}i_b + S_{c1}i_c - i_{dc}e \tag{6}$$

In equation (6), C stands for capacitance. Equation (7) is the current equation for node N.

$$C_2\frac{dU_{dc2}}{d_t} = -S_{a3}i_a + S_{b3}i_b + S_{c3}i_c - i_{dc} \tag{7}$$

Equation (8) is the equation for the midpoint Z on DC side.

$$C_1\frac{dU_{dc1}}{d_t} + C_2\frac{dU_{dc2}}{d_t} = -(S_{a2}i_a + S_{b2}i_b + S_{c2}i_c) \tag{8}$$

Therefore, the state of power switch determines the direction and magnitude of each phase's input current on AC side. The midpoint potential current in DC circuit depends on the current at neutral point Z. In order to determine the operating time and switching order of this three-level system, SVPWM was introduced into the study [20]. The SVPWM algorithm has a high accuracy and can realize the accurate control of the voltage and current of the charging pile system. At the same time, its SVPWM can generate the output voltage waveform close to the ideal sine wave, reduce the harmonic content and electromagnetic interference, and then improve the power factor and efficiency of the charging pile system. Furthermore, the algorithm can flexibly adjust the switching time and switching state of the switching device according to the input reference signal to achieve precise control of the output voltage and current. Due to the inconsistent calculation method of vector action time in traditional three-level SVPWM, a simplified three-level SVPWM based on reference voltage decomposition was introduced in the study.The simplified three-level SVPWM algorithm reduces computational complexity, improves real-time performance, and reduces hardware costs.Figure 2 shows its vector diagram.

In Figure 2, $\vec{V}_{ref}$ stands for the three-level reference voltage vector. For any $\vec{V}_{ref}$, when it is within the range of a small hexagon, it is defined as a large sector, represented by the letter S. The triangles within the hexagon are small sectors

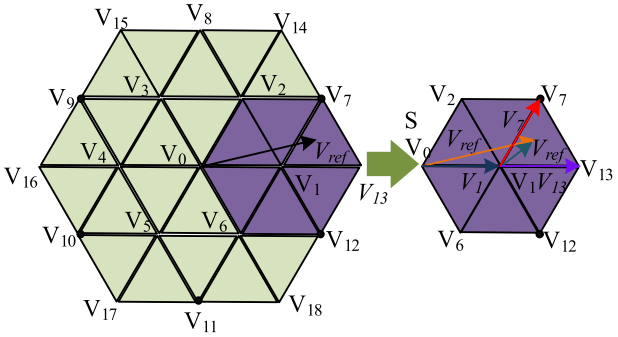

FIGURE 2. Vector diagram of three-level SVPWM algorithm based on reference voltage decomposition.

represented by the letter N. This $\vec{V}_{ref}$ can be equivalent to the sum of the voltage vector $\vec{V}_{ref}$ of a small sector and a basic vector $\vec{V}_1$ of a large sector. According to the volt second Equivalence principle and these three vector synthesis principle, formula (9) can be obtained.

$$\begin{cases} T_s \cdot \vec{V}_{ref} = T_1 \cdot \vec{V}_1 + T_7 \cdot \vec{V}_7 + T_{13} \cdot \vec{V}_{13} \\ T_s = T_1 + T_7 + T_{13} \end{cases} \tag{9}$$

In equation (9), T stands for the time constant. According to the principle of vector synthesis, equation (10) can be obtained.

$$\begin{cases} \vec{V}'_1 = \vec{V}_1 - \vec{V}_1 \\ \vec{V}'_7 = \vec{V}_7 - \vec{V}_1 \\ \vec{V}'_{13} = \vec{V}_{13} - \vec{V}_1 \\ \vec{V}'_{ref} = \vec{V}_{ref} - \vec{V}_1 \end{cases} \tag{10}$$

Introducing equation (10) into equation (9) yields equation (11).

$$\begin{cases} (\vec{V}_{ref} - V_1) = (-V) + T_7 \cdot (\vec{V}_7 - V_1) + T_{13} \cdot (\vec{V}_{13} - V_1) \\ T_s \cdot \vec{V}'_{ref} = T_1 \cdot \vec{V}'_1 + T_7 \cdot \vec{V}'_7 + T_{13} \cdot \vec{V}'_{13} \end{cases} \tag{11}$$

In summary, ACtion time of each voltage vector at the three-level is the same as that of the two-level. Therefore, the corresponding three-level vector action time can be obtained by calculating the vector time using two-level SVPWM. However, in a simplified SVPWM, each sector is a hexagonal shape that overlaps with each other, and the discrimination of this area is relatively complex. Therefore, the space vector map is usually divided into six quadrilaterals with equal area. By translating the reference voltage vector, a new two-level space voltage vector is obtained. Then, a two-level SVPWM is used to calculate the voltage vector that is closest to the reference voltage. After correcting the voltage vector, three-level SVPWM will be converted into two-level SVPWM, and the calculation of action time and the determination of switch order will also be completely based on two-level SVPWM [21].

The control of three-level AC/DC includes current inner loop control and voltage outer loop design. In the design of the current inner loop control system, it mainly executes control operations according to the instructions of the voltage outer loop system. In general, the instructions of the outer loop system can enable the three-level PWM rectifier to operate at a unit power factor state. And it can make the waveform of the output current on the grid side a sine wave. The current inner loop control system's control object is a three-phase AC time variable, and its control methods include direct and indirect current controling. Figure 3 is the control schematic diagram of SVPWM current controling method.

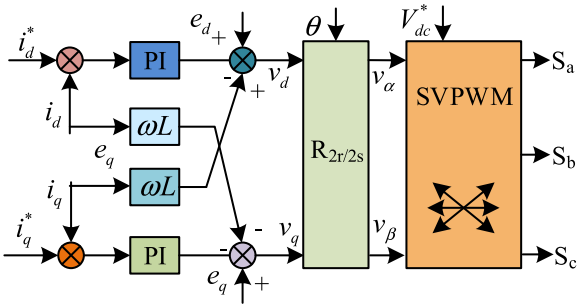

FIGURE 3. Schematic diagram of SVPWM current control method.

In Figure 3, the variables of the d-axis and p-axis can be coupled with each other, so a current feedforward decoupling method can be adopted, and a Proportional integral regulator (PI) regulator can be used to adjust id and iq without static error. In the design of voltage outer loop, voltage control mainly stabilizes DC side voltage of this three-level PWM rectifier and effectively reduces harmonics. The control method of the voltage outer loop is to first sample DC side voltage, and then feed it back to the voltage loop regulator for comparison with the reference voltage. Finally, the difference between the two was used as an instruction for current control.

B. A THREE-LEVEL BIDIRECTIONAL DC/DC CONVERTER BASED ON PHASE SHIFT MODULATION

In this three-level bidirectional DC/DC converter topology, n is the turn ratio of the transformer. The circuit topology of this converter mainly includes a high-frequency transformer and two half bridge three-level structures. These two half bridge three-level structures are located on the primary and secondary sides of the transformer. The role of high-frequency transformer is Galvanic isolation and change of voltage level. The power in this converter has two transmission directions, and its working state can be converted according to different transmission directions. When the power transmission direction of the converter is from left to right, it indicates that it is in a forward state. When the power transmission direction of the converter is from right to left, it indicates that it is in a reverse state [22]. Figure 4 shows the topology of a three-level bidirectional DC/DC converter. Among them, S1 and S4 are the main power switches, S2 and S3 are clamping circuit switches, and the four switches are located on the same bridge arm of the two bridge arms. Q1,

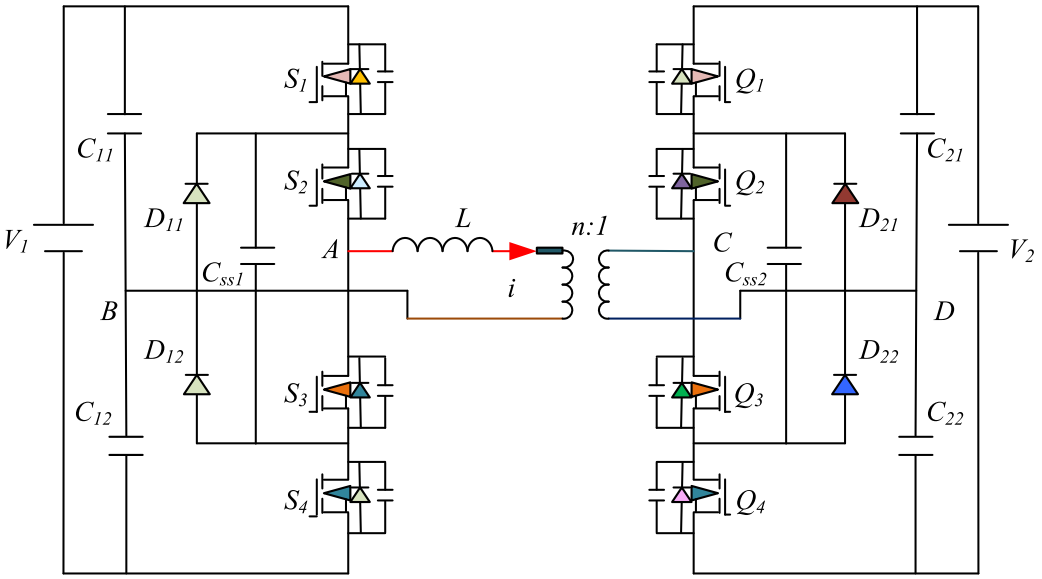

FIGURE 4. Topological structure of three-level bidirectional DC/DC converter.

Q2, Q3 and Q4 are three-level bridge arm switches, of which Q1 and Q4 are lead switches, and Q2 and Q3 are Flyback diode. Css1 stands for an active clamping capacitor, while Css2 stands for a flying capacitor.

When the converter operates in the forward state, Figure 5 shows its waveform, representing the waveform formed by this three-level bidirectional DC/DC converter under phase shift control method. From the figure, the on/off states of S1 and S2 switches are opposite to those of S3 and S4. Due to the single phase shift control adopted by the converter, the duty cycle of the switch driver signal is 0.5, and the duty cycle of output voltage on transformer's both sides is also 0.5. At the same time, there is a delay in the on/off state of the switch tubes on both sides of the converter, which means there is a phase shift angle. Each switch cycle includes 10 states. During the time period from t0 to t1, switches S1 and S2 are both in a conduction state, and DQ1 and DQ2 are also in a conduction state. At this time, the circuit is stable. During the time period t1 to t2, at time t1, S1 and S2 are disconnected, and the voltage of CS1 and CS2 increases from 0 to V1/2, while the voltage of CS3 and CS4 decreases from V1/2. During the time period t2 to t3, at time t2, DS3 and DS4 are turned on, and then S3 and S4 are in a conduction state. At this time, S3 and S4 belong to zero voltage conduction. At the same time, i continues to decrease until it reaches 0 at t3, and then the current will flow in the opposite direction. During the time period from t4 to t5, at time t4, Q1 and Q2 are at zero voltage shutdown, and DQ3 and DQ4 carry out continuous current to ensure that the current direction remains unchanged. At time t5, the voltage of CQ1 and CQ2 increases from 0 to V2/2, while the voltage of CQ1 and CQ2 decreases from V2/2 to 0. During the time period from t5 to t6, S1 and S2 are turned off at zero voltage. During the time period from t6 to t7, at time t7, S1 and S2 are in a

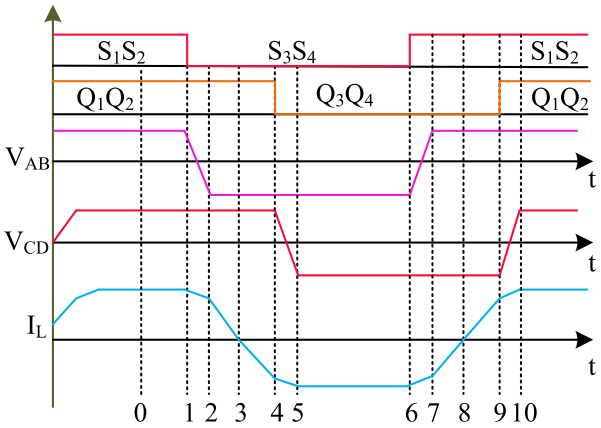

FIGURE 5. Ideal waveform of the converter in forward working state.

zero voltage conduction state, and the current continues to rise. During the time period from t8 to t9, the current at t8 changes from 0 to positive, and Q3 and Q4 are in zero voltage conduction. During the time period from t9 to t10, Q3 and Q4 at time t9 were at zero voltage shutdown, while DQ1 and DQ2 continued to flow, and the current continued to decrease. At time t10, S1 and S2 are in a zero voltage conduction state, and the on-off state of the switch returns to the time period t0∼t1, starting to enter the next cycle [23], [24]. When a three-level bidirectional DC/DC converter operates in the reverse state, its mode is relatively similar to the forward state, and it also has 10 modes in one cycle.

Soft switch is a kind of switching device that uses the resonance of capacitance and inductor in the circuit. In soft switches, the capacitance and inductors are carefully designed and arranged to form resonant circuits at specific

frequencies. When the input voltage is applied on the resonant circuit, the energy between the capacitance and the inductor is exchanged and switched at the right time. Soft switching technology reduces the change rate of current and voltage in the switching process, reduces switching noise and electromagnetic interference, and improves the anti-interference performance of the circuit. At the same time, it can reduce the energy loss in the switching process and improve the energy utilization efficiency of the system. In addition, the technology can be used in high pressure and high frequency situations to meet a wider range of application needs. This three-level bidirectional DC/DC converter soft switching used in the study is achieved through Zero Voltage Switch (ZVS), where equation (12) is the condition for the original side bridge arm to achieve soft switching.

$$I_L(\pi) \geq 0 \tag{12}$$

It can also be expressed as equation (13).

$$\phi \geq \frac{\pi(d-1)}{2d} \tag{13}$$

In equation (13), ϕ stands for the phase shift angle. d stands for the voltage gain. Among them, the range of ϕ is $-90° \leq \phi \leq 90°$. Equation (14) is the condition for the auxiliary bridge arm of the converter to achieve soft switching.

$$I_L(\phi) \geq 0 \tag{14}$$

It can also be expressed as equation (15).

$$\phi \geq \frac{\pi(1-d)}{2} \tag{15}$$

In single phase shift control, when $d = 1$, both the primary and secondary bridge arms can achieve ZVS within the ϕ range. But in the case of forward flow of converter power. When $d < 1$, the range of ZVS achieved by the secondary bridge arm will increase with the increase of voltage gain. When $d > 1$, this interval will decrease as d increases. In the case of reverse power flow, the result changes in the opposite direction. In general, the control methods for three-level bidirectional DC/DC converters include variable duty cycle and phase shift modulation. Among them, the control method of variable duty cycle is mainly achieved by changing the duty cycle of the switch driver signal to achieve control of this three-level bidirectional DC/DC converter. This control method can ultimately obtain a certain output voltage. Figure 6 shows the waveform of the on and off states of the switch under the control of this method.

In Figure 6, during the time period t1 to t2, S1 is in the off state at time t1. At this time, the inductance charges capacitor C1 and discharges C3 and C4, creating zero voltage conditions for the conduction of S3 and S4. During the time period t2 to t3, S3 is in a zero voltage conduction state, and S2 is also in a conduction state, with the output voltage level changing from +1 to 0. At time t3, S2 is in a zero current or zero voltage shutdown state. During the time period from t3 to t4, the current on the inductor flows in reverse and S3 is used to charge capacitor C4, which does not meet

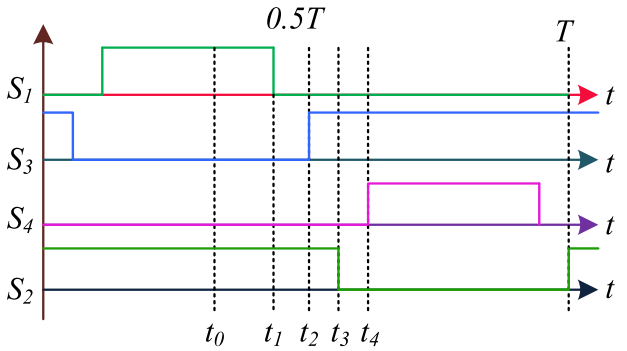

FIGURE 6. Waveform diagram of variable duty cycle control method.

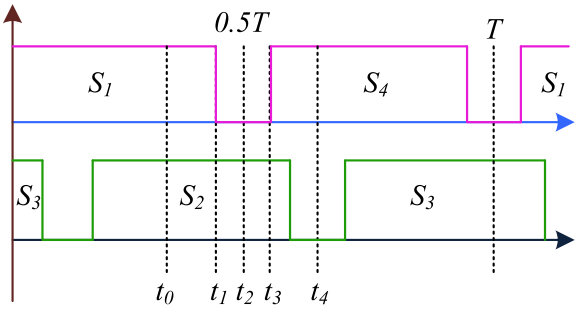

FIGURE 7. Waveform diagram of phase shift modulation control method.

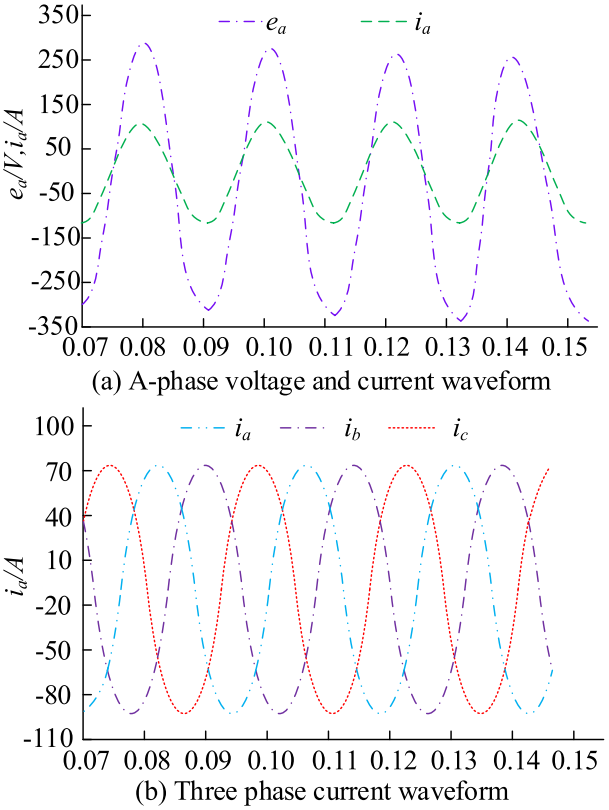

FIGURE 8. Simulation waveform of steady-state performance of three-level PWM rectifier.

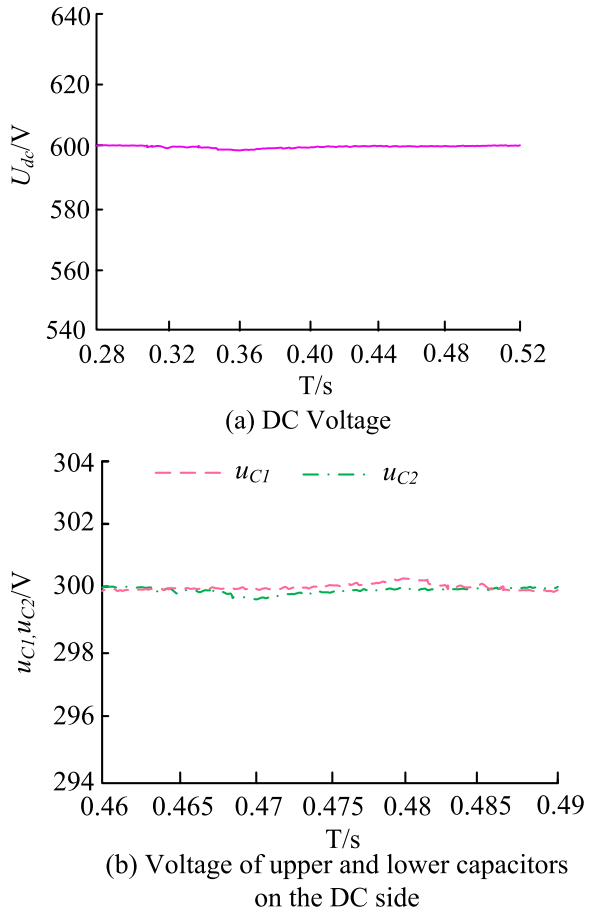

FIGURE 9. Simulation waveform of DC side voltage control.

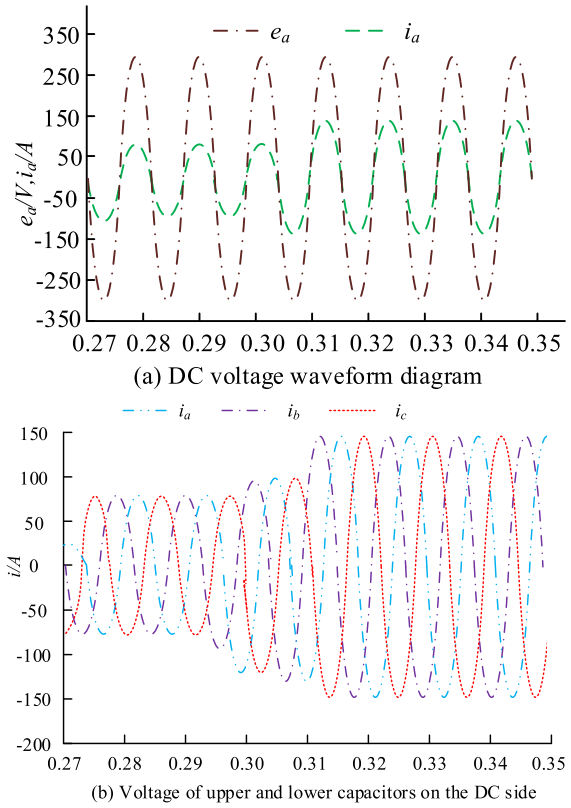

FIGURE 10. Dynamic performance simulation waveform of three-phase PWM rectifier on AC side.

the soft turn on condition. Therefore, under the control of the variable duty cycle method, this three-level bidirectional DC/DC converter can only achieve soft switching conditions for S2 and S3. The control method of phase-shifting modulation mainly sets the duty cycle of the switch tube to 0.5, and controls the duty cycle of the output voltage by shifting the driving timing of the switch tube. Figure 7 shows the waveform of the phase shift modulation control method.

In Figure 7, during the time period t1 to t2, S1 at time t1 is in the off state, and the inductance current charges capacitor C1 while discharging capacitor C4. During the time period t2 to t3, the C1 voltage at time t2 will increase. At this point, the voltage of C4 continues to discharge until the voltage value is zero, D4 enters a conduction state, and S4 enters a zero voltage conduction state. During the time period from t3 to t4, at time t3, S2 is in the off state, the inductance is charged with C2, and C3 is discharged. At time t4, the voltage of C2 continues to increase and the voltage of C3 decreases to 0. At this point, D3 enters a conduction state and S3 enters a zero voltage conduction state. Therefore, in the control method of phase shift modulation, all switches in the converter can achieve soft switching. Considering that the application of electronic systems is at high voltage and high frequency, reducing switch losses is crucial. The use of phase-shifting modulation control method can effectively solve this problem, so it is studied to apply it to the control simulation of three-level bidirectional DC/DC.

IV. THREE LEVEL AC/DC AND BIDIRECTIONAL DC/DC SIMULATION EXPERIMENTS OF PCS SUBSYSTEM

In the first section of this chapter, simulation experiments are conducted to analyze the application of simplified SVPWM in three-level PWM rectifiers, including steady-state simulation analysis and dynamic simulation analysis, to verify its effectiveness. The second section mainly conducted simulation experiments and analysis on the three-level bidirectional DC/DC converter, mainly analyzing the performance characteristics of the converter and the implementation conditions of its soft switching.

A. SIMULATION ANALYSIS OF THREE-LEVEL PWM RECTIFIER BASED ON SIMPLIFIED SVPWM

Table 1 shows the experimental parameters.

This study first conducts steady-state simulation analysis on simplified SVPWM, and the steady-state performance simulation waveform of a three-level PWM rectifier based on simplified SVPWM is shown in the figure. According to Figure 8 (a), the current and voltage phases of phase A are always synchronized, and the sine of the current is relatively

TABLE 1. Experimental parameters.

Parameter	Numerical value
Effective value of grid phase voltage	220V
DC side voltage setting value	600V
Switching frequency	5kHz
Filter inductance	1.5mH
Load resistance	10Ω
DC side capacitance	4700μF
DC side lower capacitance	4700μF

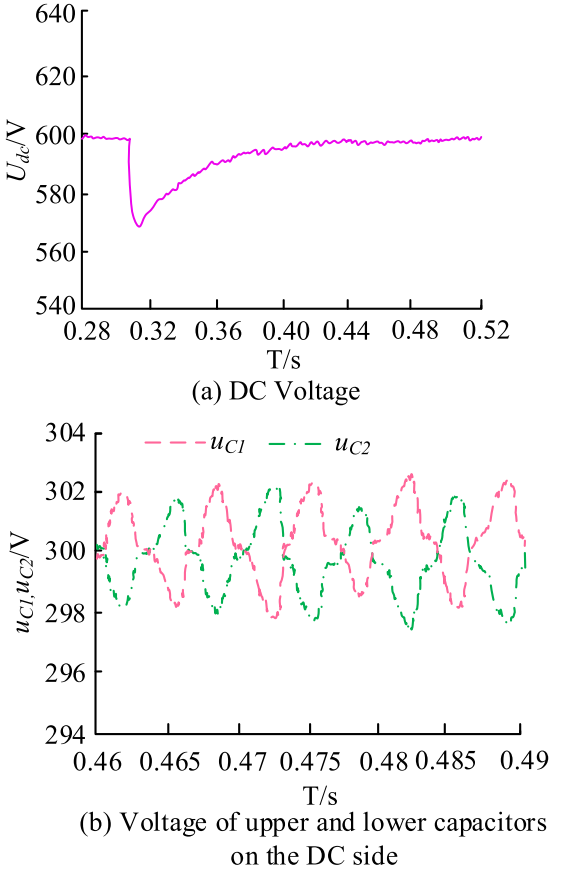

FIGURE 11. Dynamic performance simulation waveform of DC side.

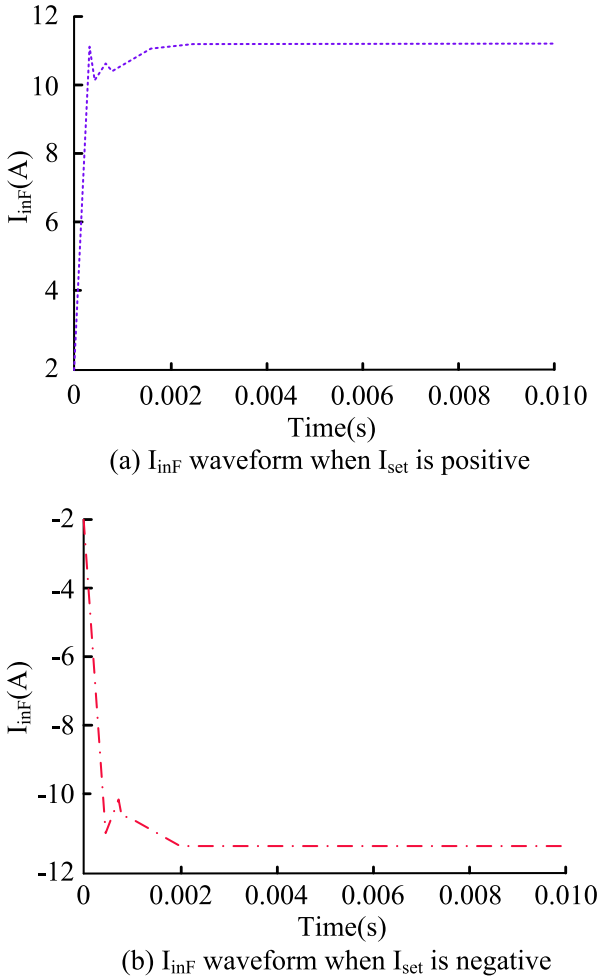

FIGURE 12. Changes in current values of IinF under different Iset.

high. This indicates that the control system can effectively achieve unit power factor operation and has a good control effect on current. At the same time, it can be seen that the maximum current value of phase A is stable at about 80A, and the maximum voltage value is stable at 300V.According to Figure 8 (b), the sine degree of three-phase current is high, the phase difference of each current is 120 °, and the maximum current value is stable at 80V.

Figure 9 shows the flow side voltage control's simulating waveform. From Figure 9(a), the voltage on DC side is stable at the given value of 600V. From Figure 9(b), the voltage of the upper and lower capacitors on DC side almost completely coincide, and both remain stable at around 300V.

This study continued to validate the dynamic performance of simplified SVPWM under sudden load changes. In the experiment, at t=0.3s, a 10 Ω load was paralleled on DC side, resulting in a load resistance of 5 Ω on DC side. Figure 10 shows the dynamic performance simulation waveform of AC side of a three-phase PWM rectifier. According to Figure 10(a), the phases of voltage and phase A current are synchronized before and after adding the load, indicating that the operating state of this system belongs to unit power factor operation. And after adding the load, the A-phase voltage value remains unchanged, and its maximum voltage value stabilizes at 300V. After adding the load, the maximum current value of phase A changes from 80A to 150A. According to Figure 10 (b), the sine of three-phase current value is high, and its phase difference is 120 °. And the maximum value of this three-phase current suddenly changes from 80A to 150A after the load is added, and continues to rise until it is stable at about 150A, indicating that the control system has a high response speed and good stability.

Figure 11 shows the simulation waveform of the dynamic performance on DC side. According to Figure 11 (a), at t = 0.3s, due to the sudden addition of the load, the voltage on DC side suddenly decreased to 570V, followed by a continuous increase in voltage value. When t = 0.42s, it rose to 600V

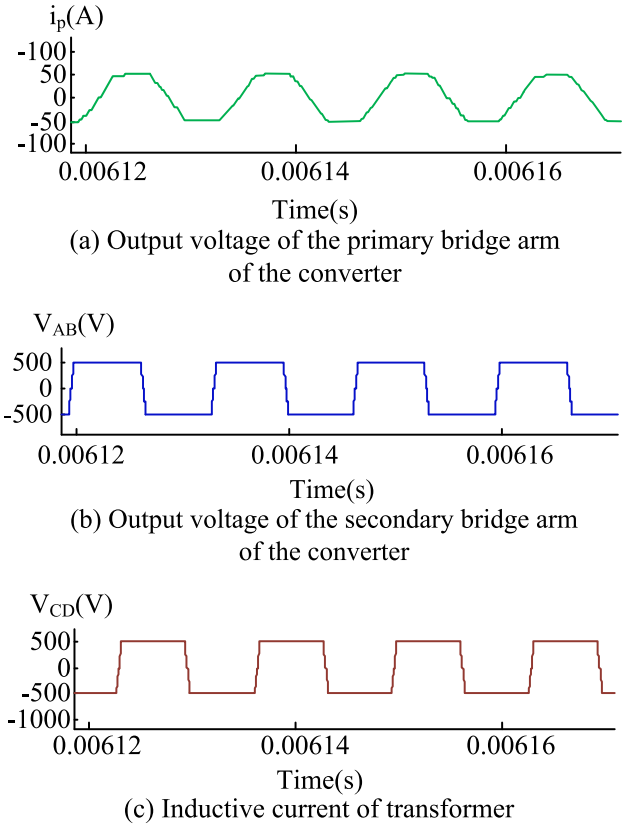

FIGURE 13. Output voltage and inductance current waveform of the bridge arms on both sides of the converter.

and stabilized around this value. According to Figure 11(b), when the load suddenly changes, the fluctuation range of the voltage of the upper and lower capacitors is around plus or minus 3V.

B. SIMULATION EXPERIMENT OF THREE-LEVEL BIDIRECTIONAL DC/DC CONVERTER

The study uses power simulation software to simulate a three-level bidirectional DC/DC converter, to analyze the implementation conditions of the converter and its soft switching. When conducting simulation analysis, the various simulation parameters of the converter are set first. Then, different I_{set} is set to change the phase shift angle of the converter, and its soft switching characteristics and current voltage stress on the switch tube were analyzed when the transmission power was constant. Table 2 shows the specific simulation parameters.

This study first explores whether this three-level bidirectional DC/DC converter can meet the bidirectional transmission of power. I_{set} is set to positive and negative directions respectively, and the current value changes of the input current I_{inF} of the primary side bridge arm are analyzed. Figure 12 shows the changes in I_{inF} under different I_{set} conditions. According to Figure 12, the waveform diagrams in both cases are relatively similar, and the maximum absolute input current of the original bridge arm is 11.5A. When the set

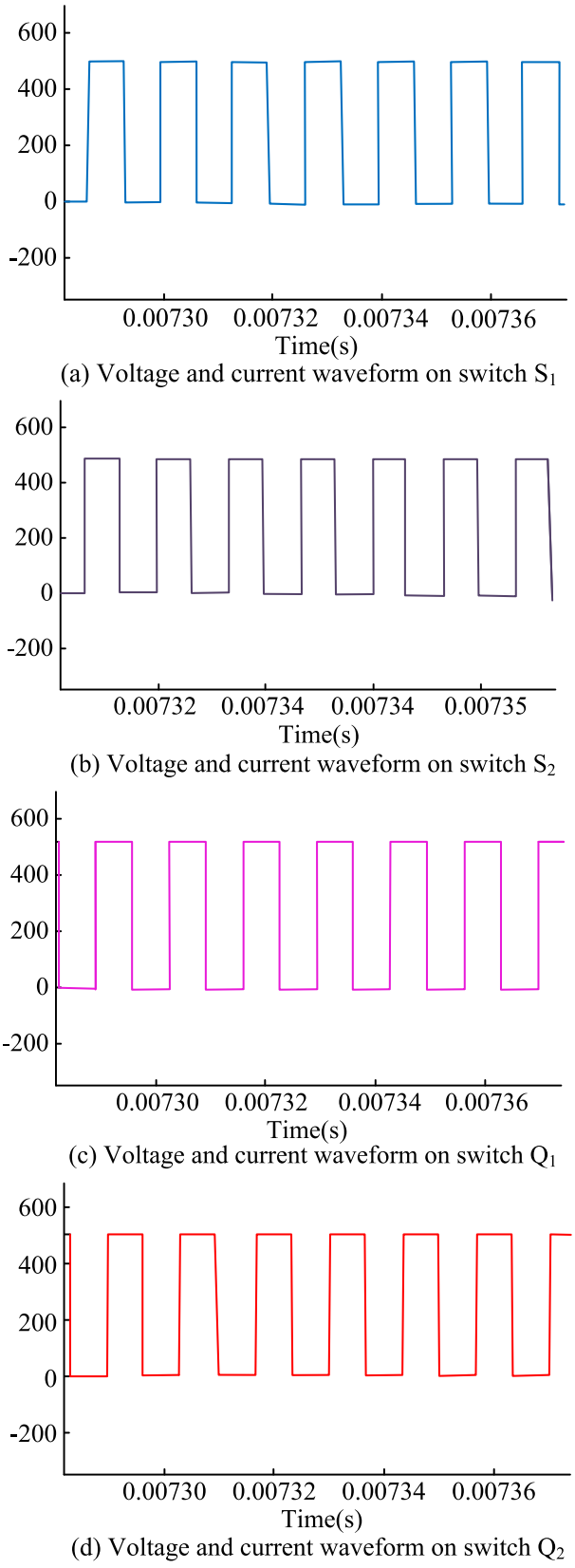

FIGURE 14. Voltage waveforms of switch tubes S1, S2, Q1, Q2.

current I_{set} is positive, the current value of the input current I_{inF} of primary bridge arm stabilizes at 11.5A around 0.025s.

TABLE 2. Simulation parameter table.

Parameter	Numerical value
Input voltage	1000V/DC
Output voltage	1000V/DC
Rated power	3kW
Switching frequency	50kHz
Clamping capacitor	220μF
Flying capacitor	220μF
Transmission inductance	60μH
Boost inductance	200μH

When the set current I_{set} is negative, the current value of the input current I_{inF} of the primary bridge arm stabilizes at -11.5A around 0.020s. This indicates that this three-level bidirectional DC/DC converter used in the study can perform bidirectional transmission.

Research continues to validate the implementation of soft switches in the converter. I_{set} is set to be greater than or equal to the limit value, with a phase shift angle of 0.25 and a phase shift angle of 90 °. Figure 13 shows the waveform of inductance current and output voltage of converter's primary and secondary bridge arms at this time. According to Figure 13, the peak current of the inductor current ofconverter is 50A, and it meets the implementation conditions of soft switching, namely $I_L(\pi) \geq 0$ and $I_L(\phi) \geq 0$. And the peak output voltage of both bridge arms is 500V, and the phase angle of the waveform differs by 90 °. As a result, all the switches in this three-level bidirectional DC/DC converter have achieved soft switching.

Figure 14 shows the voltage waveforms of switch tubes S1, S2, Q1, Q2. According to Figure 14, the switch tubes are both zero voltage on and off. And the voltage stress on each switch tube on both bridge arms is 1/2 of the input voltage and output voltage, which is 500V. In addition, the voltage fluctuation period of each switch tube is the same, and the phase angles of S1, S2 and Q1, Q2 differ by 90 °. This indicates that the three-level bidirectional DC/DC converter can effectively achieve soft switching.

V. CONCLUSION

Electric vehicle industry developing has driven the improvement of PCS technology in new energy. This study conducted relevant research on two subsystems in PCS. A simplified three-level SVPWM was used to determine the operating time of three-level AC/DC vector sector, and it was applied to the control of three-level AC/DC current inner loop and appearance design. The characteristics of this three-level bidirectional DC/DC converter and the implementation conditions of soft switching were analyzed, and the control method of phase shift modulation was adopted to control the converter. These results confirmed that in the steady-state simulation experiment of simplified SVPWM, the maximum A-phase current remained stable at around 80A, and the maximum current remained stable at 300V. And the phase of its current and voltage always remain synchronized, and the sine of current is relatively high. And the phase difference of each current of three-phase current is 120 °, and the maximum current value is stable at 80V. In addition, the voltage value on DC side is stable at 600V, and the capacitor voltage on and off DC side is stable at around 300V. In the dynamic performance analysis of simplified SVPWM, after adding a load, the voltage on DC side instantly decreases to 570V, and subsequently stabilizes at 600V. And the voltage's fluctuation range of the upper and lower capacitors on DC side is about plus or minus 3V. The simplified SVPWM has good stability and response performance in the control of three-phase PWM rectifiers. In the experiment exploring the implementation of soft switching in the converter, the peak current of the inductor current in the converter is 50A, and it meets the implementation conditions of soft switching. And the peak output voltage of both bridge arms is 500V, and the phase angle of the waveform differs by 90 °. In addition, the voltage stress on switch tubes S1, S2, Q1, and Q2 is 1/2 of the input voltage and output voltage, and they are all turned on and off at zero voltage. The application of three-level AC/DC and three-level bidirectional DC/DC converters in photovoltaic charging pile systems has advantages such as efficient performance, flexibility, and reliability. It can effectively achieve the energy conversion of photovoltaic battery packs, balance of DC buses, and charge and discharge control of electric vehicle batteries, providing stable and reliable energy support for the operation of photovoltaic charging pile systems.However, this study only conducted simulation verification on the design and did not involve it in actual research. And the influence of other parameters on the experiment was ignored in the simulation, so further work needs to be improved in this direction.

REFERENCES

[1] S. Aznavi, P. Fajri, M. B. Shadmand, and A. Khoshkbar-Sadigh, "Peer-to-peer operation strategy of PV equipped office buildings and charging stations considering electric vehicle energy pricing," *IEEE Trans. Ind. Appl.*, vol. 56, no. 5, pp. 5848–5857, Sep. 2020, doi: 10.1109/TIA.2020.2990585.

[2] N. A. El-Taweel, H. Farag, M. F. Shaaban, and M. E. AlSharidah, "Optimization model for EV charging stations with PV farm transactive energy," *IEEE Trans. Ind. Informat.*, vol. 18, no. 7, pp. 4608–4621, Jul. 2022, doi: 10.1109/TII.2021.3114276.

[3] H. Li, M. A. Azzouz, and A. A. Hamad, "Cooperative voltage control in MV distribution networks with electric vehicle charging stations and photovoltaic DGs," *IEEE Syst. J.*, vol. 15, no. 2, pp. 2989–3000, Jun. 2021, doi: 10.1109/JSYST.2020.3001040.

[4] A. Ehsan and Q. Yang, "Active distribution system reinforcement planning with EV charging stations—Part I: Uncertainty modeling and problem formulation," *IEEE Trans. Sustain. Energy*, vol. 11, no. 2, pp. 970–978, Apr. 2020, doi: 10.1109/TSTE.2019.2915338.

[5] K.-H. Tan, F.-J. Lin, C.-M. Shih, and C.-N. Kuo, "Intelligent control of microgrid with virtual inertia using recurrent probabilistic wavelet fuzzy neural network," *IEEE Trans. Power Electron.*, vol. 35, no. 7, pp. 7451–7464, Jul. 2020, doi: 10.1109/TPEL.2019.2954740.

[6] M. Mansoor, M. Stadler, H. Auer, and M. Zellinger, "Advanced optimal planning for microgrid technologies including hydrogen and mobility at a real microgrid testbed," *Int. J. Hydrogen Energy*, vol. 46, no. 37, pp. 19285–19302, May 2021, doi: 10.1016/j.ijhydene.2021.03.110.

[7] Z. Huang and A. Mu, "Research and analysis of performance improvement of vanadium redox flow battery in microgrid: A technology review," *Int. J. Energy Res.*, vol. 45, no. 10, pp. 14170–14193, Apr. 2021, doi: 10.1002/er.6716.

[8] F. Yang, X. Feng, and Z. Li, "Advanced microgrid energy management system for future sustainable and resilient power grid," *IEEE Trans. Ind. Appl.*, vol. 55, no. 6, pp. 7251–7260, Nov. 2019, doi: 10.1109/TIA.2019.2912133.
[9] L. Yavuz, A. Önen, S. M. Muyeen, and I. Kamwa, "Transformation of microgrid to virtual power plant—A comprehensive review," *IET Gener., Transmiss. Distrib.*, vol. 13, no. 11, pp. 1994–2005, Feb. 2019, doi: 10.1049/iet-gtd.2018.5649.
[10] S. Chandak and P. K. Rout, "The implementation framework of a microgrid: A review," *Int. J. Energy Res.*, vol. 45, no. 3, pp. 3523–3547, Mar. 2021, doi: 10.1002/er.6064.
[11] T. M. Masaud and E. F. El-Saadany, "Correlating optimal size, cycle life estimation, and technology selection of batteries: A two-stage approach for microgrid applications," *IEEE Trans. Sustain. Energy*, vol. 11, no. 3, pp. 1257–1267, Jul. 2020, doi: 10.1109/TSTE.2019.2921804.
[12] P. Prem, P. Sivaraman, J. S. S. S. Raj, M. J. Sathik, and D. Almakhles, "Fast charging converter and control algorithm for solar PV battery and electrical grid integrated electric vehicle charging station," *Automatika*, vol. 61, no. 4, pp. 614–625, Aug. 2020, doi: 10.1080/00051144.2020.1810506.
[13] M. Shin, D.-H. Choi, and J. Kim, "Cooperative management for PV/ESS-enabled electric vehicle charging stations: A multiagent deep reinforcement learning approach," *IEEE Trans. Ind. Informat.*, vol. 16, no. 5, pp. 3493–3503, May 2020, doi: 10.1109/TII.2019.2944183.
[14] S. Praveenkumar, E. B. Agyekum, J. D. Ampah, S. Afrane, V. I. Velkin, U. Mehmood, and A. A. Awosusi, "Techno-economic optimization of PV system for hydrogen production and electric vehicle charging stations under five different climatic conditions in India," *Int. J. Hydrogen Energy*, vol. 47, no. 90, pp. 38087–38105, Nov. 2022, doi: 10.1016/j.ijhydene.2022.09.015.
[15] S. M. Shariff, M. S. Alam, F. Ahmad, Y. Rafat, M. S. J. Asghar, and S. Khan, "System design and realization of a solar-powered electric vehicle charging station," *IEEE Syst. J.*, vol. 14, no. 2, pp. 2748–2758, Jun. 2020, doi: 10.1016/j.ijhydene.2022.09.015.
[16] A. Sierra, C. Gercek, K. Geurs, and A. Reinders, "Technical, financial, and environmental feasibility analysis of photovoltaic EV charging stations with energy storage in China and the United States," *IEEE J. Photovolt.*, vol. 10, no. 6, pp. 1892–1899, Nov. 2020, doi: 10.1109/JPHOTOV.2020.3019955.
[17] M. Zand, M. A. Nasab, P. Sanjeevikumar, P. K. Maroti, and J. B. Holm-Nielsen, "Energy management strategy for solid-state transformer-based solar charging station for electric vehicles in smart grids," *IET Renew. Power Gener.*, vol. 14, no. 18, pp. 3843–3852, Dec. 2020, doi: 10.1049/iet-rpg.2020.0399.
[18] A. Verma and B. Singh, "Multimode operation of solar PV array, grid, battery and diesel generator set based EV charging station," *IEEE Trans. Ind. Appl.*, vol. 56, no. 5, pp. 5330–5339, Sep. 2020, doi: 10.1109/TIA.2020.3001268.
[19] S. Sharma and Y. R. Sood, "Microgrids: A review of status, technologies, software tools, and issues in Indian power market," *IETE Tech. Rev.*, vol. 39, no. 2, pp. 411–432, Mar. 2022, doi: 10.1080/02564602.2020.1850367.
[20] S. Fang, Y. Wang, B. Gou, and Y. Xu, "Toward future green maritime transportation: An overview of seaport microgrids and all-electric ships," *IEEE Trans. Veh. Technol.*, vol. 69, no. 1, pp. 207–219, Jan. 2020, doi: 10.1109/TVT.2019.2950538.
[21] D. Yan, H. Yin, T. Li, and C. Ma, "A two-stage scheme for both power allocation and EV charging coordination in a grid-tied PV–battery charging station," *IEEE Trans. Ind. Informat.*, vol. 17, no. 10, pp. 6994–7004, Oct. 2021, doi: 10.1109/TII.2021.3054417.
[22] S. Singh, V. B. Pamshetti, and S. P. Singh, "Time horizon-based model predictive Volt/VAR optimization for smart grid enabled CVR in the presence of electric vehicle charging loads," *IEEE Trans. Ind. Appl.*, vol. 55, no. 6, pp. 5502–5513, Nov. 2019, doi: 10.1109/TIA.2019.2928490.
[23] M. Yang, "Research on vehicle automatic driving target perception technology based on improved MSRPN algorithm," *J. Comput. Cognit. Eng.*, vol. 1, no. 3, pp. 147–151, Jan. 2022, doi: 10.47852/bonviewJCCE20514.
[24] Y. Guo, Z. Mustafaoglu, and D. Koundal, "Spam detection using bidirectional transformers and machine learning classifier algorithms," *J. Comput. Cognit. Eng.*, vol. 2, pp. 5–9, Apr. 2022, doi: 10.47852/bonviewJCCE2202192.

YANSHENG HUANG was born in Guangxi, China, in 1978. He received the degree from the School of Mechanical Engineering, Guangxi University, in 2002, and the master's degree in electrical from the Wuhan University of Technology, Hubei, China, in 2013.

Since 2008, he has been a Teacher with the School of Energy Power and Environmental Engineering, Guangxi Electrical Polytechnic Institute. He has authored and published one textbook as the first Editor-in-Chief, participated in the editing and publishing of three textbooks, and published three papers. His research interests include the operation and control of thermal power generation technology and new energy generation technology.

SHUTING LIN was born in Guangxi Zhuang, China, in 1983. She received the bachelor's degree in thermal energy and power engineering from Nanjing Normal University, China, in 2006, and the master's degree in electrical engineering from Chongqing University, China, in 2015.

Since 2006, she has been a full-time Teacher with the Guangxi Electrical Polytechnic Institute, China, engaged in research and teaching of thermal power equipment application and control technology.

HAIJUN MO was born in Guangxi, China, in 1979. She received the Ph.D. degree in power engineering from Shanghai Jiao Tong University, in 2016. Since 2005, she has been a Teacher with the School of Mechanical Engineering, Guangxi University, engaged in research and teaching of computational fluid dynamics, internal combustion engine design, and internal combustion engine emission and control. She is a Lecturer.